applied sciences

MDPI

Article

Preparation of Magnetically Driven Nickel Phosphide Nanowires and Their Electrochemical Properties

Hye-Won Kim and Heon-Cheol Shin *

School of Materials Science and Engineering, Pusan National University, Busan 46241, Korea; duckgg4666@daum.net

* Correspondence: hcshin@pusan.ac.kr; Tel.: +82-515-103-099; Fax: +82-515-120-528

Abstract: In this study, nickel phosphide nanowires with various structures and compositions were fabricated for the first time via magnetically-assisted liquid phase synthesis. The curvature and aspect ratio of the nanowires largely depended on the strength of the magnetic field applied during synthesis. Their phosphorus content together with the morphology were significantly modified according to the pH and reducing agent concentration. Nanowires with different structures and phosphorus contents were preliminarily tested for their capabilities to serve in general electrochemical applications. The degree of reaction (i.e., amount of reaction charge) increased with increases in the reaction area and phosphorus content of the nanowires. The rate characteristics of the reaction showed a peculiar increasing trend for a small reaction surface area and low phosphorus content. A change in the ohmic overpotential according to the nanowire curvature (aspect ratio) and porosity was suggested to be the reason for this unusual trend. Electrodes with high phosphorus contents or high reaction surface areas rapidly deteriorated during repetitive redox reactions. Based on the results for the degradation degree, the effect of the reaction surface area dominated that of the phosphorus content in the deterioration of the nickel phosphide nanowires.

Keywords: liquid phase synthesis; magnetic field; nickel phosphide; nanowire; electrochemical property

Citation: Kim, H.-W.; Shin, H.-C. Preparation of Magnetically Driven Nickel Phosphide Nanowires and Their Electrochemical Properties. *Appl. Sci.* **2022**, *12*, 49. https://doi.org/10.3390/app12010049

Academic Editor: Daniel Munteanu

Received: 19 November 2021
Accepted: 17 December 2021
Published: 21 December 2021

1. Introduction

Transition metal phosphides have beneficial physical, chemical, and mechanical properties owing to their excellent electronic conductivity [1] and stability in acidic and alkaline conditions [2], as well as a high melting point, hardness, and abrasion resistance [3]. In addition, the coexistence of metal–metal, metal–phosphorus, and phosphorus–phosphorus bonds make it possible to synthesize transition metal compounds of various stoichiometries, compositions, and crystal structures. Accordingly, there have been many studies to apply these compounds to engineering applications, and nickel phosphides have emerged as notable candidates [4–7]. In particular, research has been actively conducted on using nickel phosphides as electrodes for different electrochemical devices such as catalysts for hydrogen and oxygen generation [8], electrodes for secondary lithium batteries [9], and electrodes for supercapacitors [10–13].

Many studies have been conducted to improve the output and efficiency of electrochemical devices by fabricating electrodes using nanomaterials. Because such electrodes possess a large surface area, the surface reaction resistance is significantly reduced. Accordingly, the reaction overpotential can be reduced, enabling high-rate and high-efficiency operation of the device. Nickel phosphide nanomaterials are synthesized by various methods, such as pyrolysis of organometallic precursors [14,15], high-temperature reduction [16,17], solid-state phase transformation [18], and the vapor–liquid–solid (VLS) method [19,20]. However, because the phosphorus precursors used for pyrolysis are expensive, flammable, and toxic, the synthesis of nanoparticles is still challenging. High-temperature reduction and solid-state phase transformation also incur high production costs due to synthesis at high temperatures. In addition, with the VLS method, it is challenging to remove the liquid

capsule that is formed during the process, and high temperatures are required. Hence, it is of high engineering significance to develop a cost-effective and highly safe method for synthesizing nickel phosphide nanomaterials. In this regard, a recent study on the synthesis of pure nickel nanostructures by liquid phase chemical reduction is noteworthy, where nickel nanoparticles were relatively quickly, inexpensively, and safely synthesized by chemical reduction. In particular, pure nickel nanowires could be synthesized without a catalyst or template due to the ferromagnetic properties of nickel in a magnetic field [21,22].

In this study, we present our preliminary results on nickel phosphide nanowires with various structures and compositions, prepared by liquid phase synthesis in a magnetic field. The phosphorus content and nanowire shape of the nickel phosphides according to synthesis conditions (i.e., the solution pH, reducing agent concentration, and magnetic field strength) were analyzed. In addition, the pure nickel phosphide electrodes were fabricated without binder and conducting agents, which might possibly distort the inherent properties, to test their intrinsic electrochemical properties. In particular, we focused on the ratio of nickel to phosphorus, the effect of the reaction surface area on the reaction degree, and the effect of the nanowire shape and structure on the reaction rate and reaction-induced material degradation.

2. Experimental Procedure

2.1. Preparation of Nickel Phosphide Nanowires

To prepare nickel phosphide nanowires, electrolyte solutions were prepared by mixing two aqueous solutions, A and B, at room temperature. Aqueous solution A was prepared by mixing various concentrations of sodium hypophosphite (a reducing agent, Sigma-Aldrich, St. Louis, MI, USA, anhydrous, 98–101%) in a mixed aqueous solution containing nickel sulfate (0.1 M, Junsei, Tokyo, Japan, 98.0%), ammonium chloride (0.34 M, Junsei, Tokyo, Japan, 98.5%), and trisodium citrate dihydrate (27 mM, a surfactant, Junsei, Japan, 99%). The pH was adjusted using sodium hydroxide (Junsei, Tokyo, Japan, 97%). Aqueous solution A was classified into two types as follows (Table 1): (1) solutions in which the pH and reducing agent concentration are fixed to investigate the effect of the magnetic field strength (samples 0L, 2L, and 18L in Table 1) and (2) solutions in which the magnetic field strength is fixed to investigate the effect of pH and the reducing agent (samples 18L, 18M, and 18H in Table 1). Aqueous solution B contained palladium chloride (1.7 mM, Sigma-Aldrich, St. Louis, MI, USA, 99%) as a nucleating agent, and the solution pH was adjusted to 2 using hydrochloric acid (Junsei, Tokyo, Japan, 99.5%).

Table 1. Preparation conditions of nickel phosphide nanowires.

Sample Name	Concentration of Sodium Hypophosphite (M)	pH	Magnetic Field Strength (mT)
0L	0.15	11	0
2L	0.15	11	2
18L	0.15	11	18
18M	0.5	9	18
18H	1	7	18

After mixing 50 mL of aqueous solution A and 3 mL of aqueous solution B, the resulting solution was heated for approximately 1 h at 70 °C to form nickel phosphide nuclei (the color of the electrolyte changed from green to black). Subsequently, a magnetic field was applied for approximately 4 min to grow them into nanowires. The magnetic field strength was controlled by changing the distance between two neodymium magnets located at both ends of the beaker containing the mixed aqueous solution and was measured using a Gauss meter (TM-801, Kanetec, Tokoyo, Japan). When the distances between the two magnets were 5 cm and 15 cm, magnetic fields of 18 mT and 2 mT, respectively, were incident on the center of the beaker under the cell configuration used in this study. After the experiment, the nickel phosphide nanowires that formed in the center of the beaker were

collected and washed with ethanol. The composition, shape, and crystal structure of the synthesized nickel phosphides were confirmed by energy-dispersive X-ray spectroscopy (EDS, 51-XMZ1004, Oxford instruments, Oxford, UK), field-emission scanning electron microscopy (FE-SEM, MIRA3, TESCAN, Brno, Czech Republic), and X-ray diffraction (XRD, Ultima-IV Rigaku, Tokoyo, Japan), respectively.

2.2. Evaluation of Electrochemical Properties of Nickel Phosphide Nanowire Electrodes

The fabricated nickel phosphide nanowires were tested as electrodes for redox systems. Nickel foam (Invisible Inc., Gyeonggi-do, South Korea, 99.5%) was used as a substrate, and ultrasonic cleaning was performed in ethanol for 1 h to remove surface impurities. An electrode was prepared by applying a pressure of 1 MPa after placing the nickel nanowires on the nickel foam substrate. Here, the additives (e.g., binder or conductive material) were not used to confirm the unique characteristics of the synthesized materials.

A three-electrode beaker cell was constructed to evaluate the electrochemical properties of the electrode and understand the intrinsic properties of the nanowires. The fabricated electrode was used as a working electrode. Platinum foil and a Hg/HgO electrode were selected as a counter and a reference electrode, respectively. A 2 M KOH aqueous solution was used as an electrolyte. To understand the basic characteristics of the electrode and estimate the amount of reaction charge, cyclic voltammetry was performed at a scan rate of 5 mV/s in the potential range of 0.2–0.6 V vs. Hg/HgO, and the rate characteristics of the reaction were estimated under various current densities ranging from 0.5 to 4 A/g. A constant cathodic/anodic current density of 3 A/g was applied 500 times to evaluate the degree of deterioration during the repetitive redox cycles.

The electrochemical active surface area (ECSA) was determined through the "capacitance method" [23,24]. For this purpose, cyclic voltammetry was performed on the prepared electrodes in a 0.1 M KOH electrolyte. At this time, the potential range corresponded to that of the open circuit potential (OCP) ± 50 mV, and the scan rates were set to 5–400 mV/s. The ECSA per unit mass was determined according to the following equations:

$$I_c = I_{\text{anodic (OCP}-50\text{mV)}} - I_{\text{cathodic (OCP}+50\text{mV)}} \quad (1)$$

$$\text{ECSA} = \frac{C_{dl}}{c \cdot m} = \frac{1}{c \cdot m} \cdot \frac{\Delta I_c}{\Delta v} \quad (2)$$

where I_C is the charging current at a specific scan rate obtained through cyclic voltammetry; $I_{\text{anodic(OCP} - 50\text{mV)}}$ and $I_{\text{cathodic(OCP} + 50\text{mV)}}$ denote the current values at OCP − 50 mV and OCP + 50 mV, respectively; C_{dl} is the double-layer capacitance, determined through the slope ($\Delta I_c/\Delta v$) of the charging current vs. the scan rate plot; c denotes the specific charge density (40 μF/cm^2 [23,24]); and m denotes the mass of nickel phosphide. All electrochemical experiments were performed using a Solartron 1470E potentiostat (AMETEK Scientific Instruments, West Sussex, UK).

3. Results and Discussion

3.1. Effect of Magnetic Field Strength on the Composition and Structure of Nickel Phosphide

The difference in the composition and structure of the nickel phosphides according to the magnetic field strength was analyzed (Samples 0L, 2L, 18L in Table 1). Figure 1a–c show the electron micrographs of nickel phosphides obtained at magnetic fields of 0, 2, and 18 mT, respectively (hereafter, each specimen is denoted as sample 0L, sample 2L, or sample 18L, where the numbers represent the magnetic field strength and the letter L indicates a low phosphorus content). In the absence of a magnetic field, the agglomeration between particles was very irregular, and the overall structure was severely bent (sample 0L, Figure 1a). However, when a magnetic field was applied, the irregular and curved growth pattern changed to a one-dimensional growth pattern, even with a relatively low magnetic field (sample 2L, Figure 1b). Nanowires with highly uniform diameters and high aspect ratios grew under a high magnetic field (sample 18L, Figure 1c). It is considered that

the wire growth of nickel phosphides in a magnetic field occurs due to the ferromagnetic properties of nickel. Nickel phosphide nanoparticles containing a large amount of nickel are arranged in a line along the magnetic flux under a magnetic field and combine to grow into nanowires. Because of the natural convection effect of the solution during synthesis, the stronger the magnetic field, the better the definition of the nanowire formed; this is consistent with previous literatures on the synthesis of pure nickel nanowires in a magnetic field [21,22].

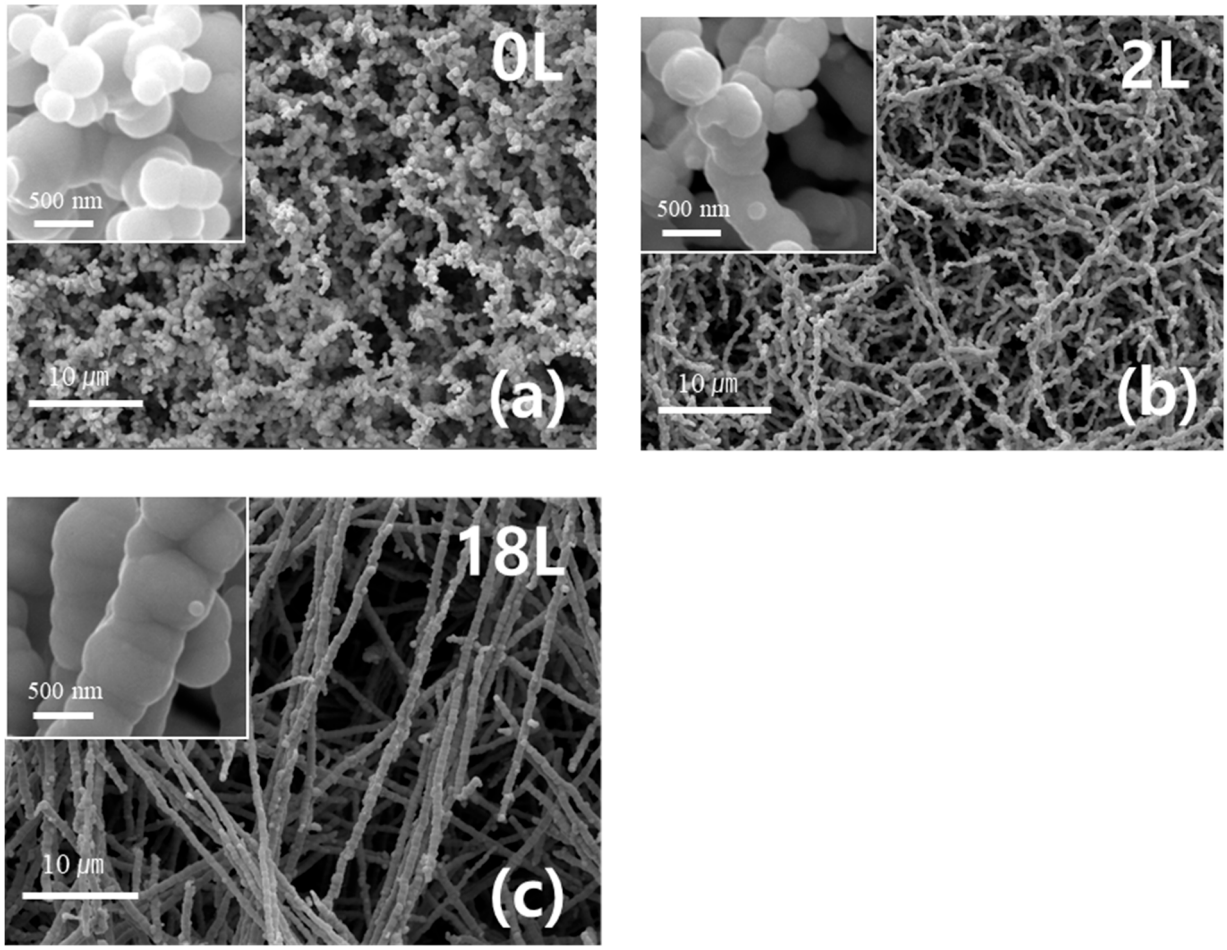

Figure 1. Scanning electron micrographs of the nickel phosphide nanowires prepared at different values of magnetic field strength: (**a**) sample 0L, (**b**) sample 2L, and (**c**) sample 18L in Table 1. Inset figures are the magnified images.

Figure 2a–c show the composition analysis results for samples 0L, 2L, and 18L, respectively. The phosphorus content in the three specimens was approximately 7–8% when the effect of oxygen resulting from surface oxidation caused by atmospheric exposure of the specimen after synthesis was eliminated. This implies that the magnetic field has virtually no effect on the composition. In addition, only broad peaks arising from the presence of Ni appear in the X-ray diffraction pattern, suggesting that the synthesized nickel phosphides are amorphous or low-crystalline materials. It is known that when the phosphorus content is relatively low, the crystallinity of nickel phosphides is sensitive to the phosphorus content. According to literature on the synthesis of nickel phosphides by electroless plating [25,26], nickel phosphides are crystalline when the phosphorus content is very low, but they become increasingly amorphous as the phosphorus content is increased. When the phosphorus content is 10 wt% or more, they are completely amorphous. Thus,

the composition and structure analysis results for the nickel phosphides synthesized in this study are consistent with those in existing literature.

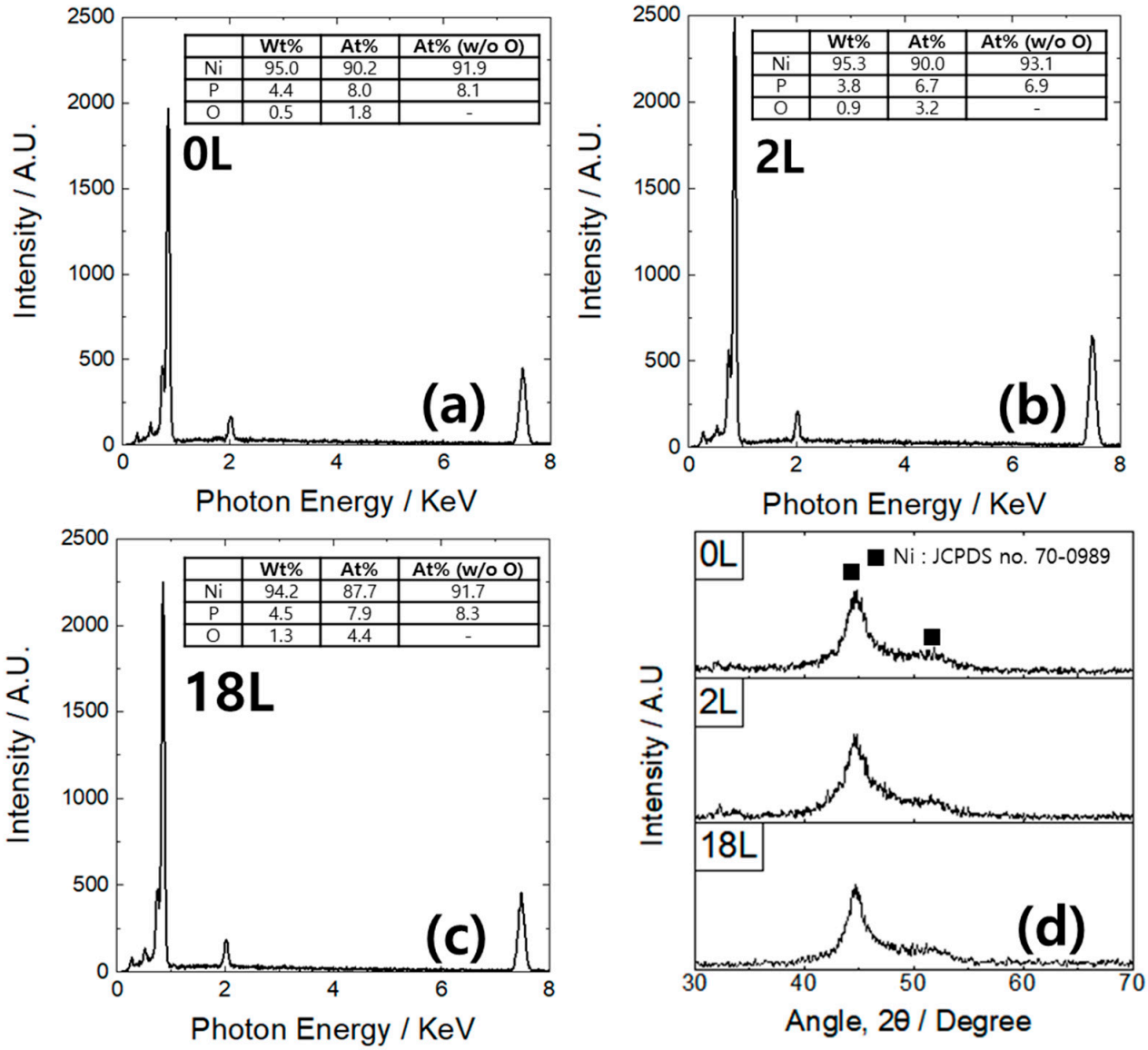

Figure 2. EDS spectra together with chemical composition ratios of the nickel phosphide nanowires prepared at different values of magnetic field strength: (**a**) sample 0L, (**b**) sample 2L, and (**c**) sample 18L from Table 1; and (**d**) their XRD patterns.

3.2. Effect of pH and Reducing Agent on the Composition of Nickel Phosphide

Nickel phosphide is typically synthesized according to the following chemical reactions [27,28].

$$(NiR_n)^{2+} + H_2PO_2^- + 3OH^- \rightarrow Ni + HPO_3^{2-} + 2H_2O + nR \quad (3)$$

$$H_2PO_2^- + 2H^+ + e^- \rightarrow P + 2H_2O \quad (4)$$

Here, R denotes a salt (generally succinate or pyrophosphate). A complex of a salt and nickel $(NiR_n)^{2+}$ is reduced by $H_2PO_2^-$ derived from a reducing agent (e.g., sodium hypophosphite). The concentrations of the Ni source and reducing agent and the pH directly affect the phosphorus and nickel contents in the product after chemical reduction.

As shown in reaction Equations (3) and (4), the phosphorus and nickel contents in nickel phosphide are directly affected by the pH and reducing agent concentration during chemical reduction. When the pH is increased, reaction (3) acts to increase the nickel content and decrease the phosphorus content, and reaction (4) is suppressed. On the other hand, the phosphorus content increases when the reducing agent concentration increases because the reducing agent is a phosphorus precursor [27]. In this study, we tried to obtain nickel phosphides with three different nickel:phosphorus composition ratios using a combination of pH levels and reducing agent concentrations (Samples 18L, 18M, and 18H in Table 1. Sample 18L is the same as sample 18L in Section 3.1. Here, M denotes a medium phosphorus content, and H denotes a high phosphorus content). The magnetic field strength was fixed at 18 mT, the value at which the nanowires were best formed in Section 3.1.

The shapes of the synthesized nickel phosphide nanowires are shown in Figure 1c (sample 18L) and Figure 3a,b (samples 18M and 18H, respectively), and the contents of nickel and phosphorus are summarized in Figure 3c. With regard to the composition, the lower the pH and higher the reducing agent concentration, the higher the proportion of phosphorus in the nickel phosphide, as discussed above. In addition, with an increase in the proportion of phosphorus, the nickel phosphide particle sizes became non-uniform, particle aggregation around the nanowire became apparent, and the aspect ratio of the nanowires decreased. It is quite likely that the changes in the nanowire shape according to the phosphorus content are related to the magnetization of nickel phosphides. The magnetization of nickel phosphides in a fixed magnetic field decreased as the phosphorus content increased or nickel content decreased, resulting in non-uniform nanowires and their small aspect ratio. Based on the structure analysis (Figure 3d), no clear crystallinity was observed in all specimens.

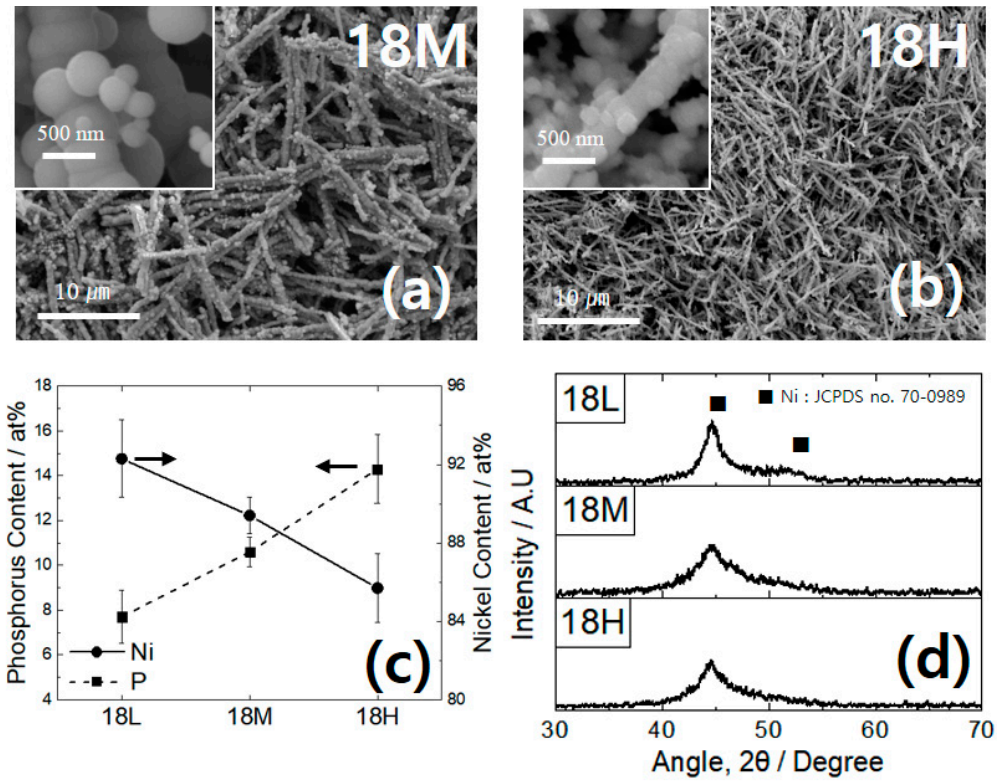

Figure 3. Scanning electron micrographs of the nickel phosphide nanowires prepared at different combinations of pH and reducing agent content: (**a**) sample 18M and (**b**) sample 18H in Table 1. Inset figures are the magnified images. (**c**) Phosphorus and nickel contents in the samples obtained from the EDS analysis and (**d**) their XRD patterns.

3.3. Electrochemical Tests

Several studies have reported the redox reaction mechanism of nickel phosphides in an aqueous solution [29–33]; however, there is still no solid consensus as to the redox reaction mechanism of nickel phosphides in an aqueous solution, except for the active participation of hydroxyl ions in the reaction. It is suggested that the following irreversible (Equation (5)) and reversible (Equation (6)) reactions take place when nickel phosphides are in an alkaline solution.

$$Ni_xP_y + xOH^- \rightarrow Ni_xP_y(OH)_x + xe^- \quad (5)$$

$$Ni_xP_y(OH)_x + xOH^- \leftrightarrow Ni_xP_yO_x + xH_2O + xe^- \quad (6)$$

Based on the reaction mechanism, it is evident that the reaction degree is increased when the interfacial reaction area between the nickel phosphide and the electrolyte is increased or when the phosphorus content in the nickel phosphide is increased.

First, we attempted to investigate the effect of the reaction area in a situation where the phosphorus content in the nickel phosphide nanowire was fixed. To this end, the characteristics of electrodes constructed with nickel phosphide nanowires (samples 0L, 2L, and 18L; 7~8 at% P (Figure 2)) obtained under various magnetic fields were analyzed. Figure 4a,b show the cyclic voltammograms in the first and the second cycles. Figure 4c presents a charging current vs. scan rate plot and the ECSA values determined based on the plot (the table inserted in the figure). The presence of the irreversible anodic reaction (Equation (5)) was confirmed by the comparison of the first and the second cyclic voltammograms: Anodic current during the first cycle (Figure 4a) was much larger than that during the second cycle (Figure 4b) throughout the entire potential range, while the cathodic current values during the first and the second cycles are almost the same, strongly indicative of the irreversible anodic process in the first cycle.

A redox peak due to the reversible reaction between nickel phosphides and hydroxyl ions (Equation (6)) was also observed in the cyclic voltammogram (Figure 4b). Notably, the electrode (sample 0L) constructed with nanowires obtained in the absence of a magnetic field exhibited the highest reaction degree (i.e., the amount of reaction charge). As the magnetic field increased, the reaction degree was decreased in sample 2L, followed by sample 18L. Based on a quantitative analysis through the cyclic voltammograms, the charge amounts transferred during cathodic reaction of samples 0L, 2L, and 18L were 31.7, 22.8, and 19.4 C/g, respectively (that is, the charge amount ratio is 0L:2L:18L = 1:0.72:0.61). On the other hand, based on Figure 4c, the ECSA values were determined to be 8036, 5550, and 4998 cm^2/g, respectively, through a capacitance method and the ratio was 1:0.69:0.62. This was approximately the same as the charge amount ratio obtained from the cyclic voltammograms. This result strongly indicates that the degree of reaction (i.e., reaction charge amount) is determined according to the reaction surface area when the phosphorus content in the nickel phosphide is the same. In other words, with respect to the reaction degree itself, heavily bent (i.e., poorly defined) nanowires fabricated in the absence of a magnetic field show high value by having a large active surface area. In contrast, well-defined nanowires fabricated under a high magnetic field show a relatively low value by having a relatively low active surface area.

Next, the characteristics of electrodes fabricated using three nanowire specimens having different phosphorus contents (samples 18L, 18M, and 18H) were compared to investigate the effect of the phosphorus content in the nickel phosphide nanowires. Figure 5a,b show the cyclic voltammograms in the first and the second cycles. Figure 5c presents a charging current vs. scan rate plot and the ECSA values determined based on the plot (the table inserted in the figure). The amounts of reaction charge were increased in the increasing order of the phosphorus content in the nickel phosphide in the cyclic voltammograms (Figure 5a,b). Based on the quantitative analysis of the reversible cyclic voltammograms (Figure 5b), the charge amounts transferred during cathodic reaction of samples 18L, 18M, and 18H were determined to be 19.4, 52.6, and 95.9 C/g, respectively

(i.e., the charge amount ratio is 18L:18M:18H = 1:2.47:4.94). In addition, the ECSA values determined based on Figure 5c were 4998, 8540, and 12,123 cm^2/g, respectively, and the ratio was 1:1.71:2.43, which is significantly different from the charge amount ratio obtained from the cyclic voltammograms. This implies that the charge amount is affected by other factors, apart from the surface area effect. Remarkably, the ratio after simple mathematical correction of the area effect is calculated to be 1:1.44:2.03, which is almost similar to the phosphorus content ratio of the specimen (7.7:10.6:14.3 = 1:1.37:1.85 in Figure 3c). These results suggest that the phosphorus content and the surface area are two main governing factors affecting the reaction charge amount.

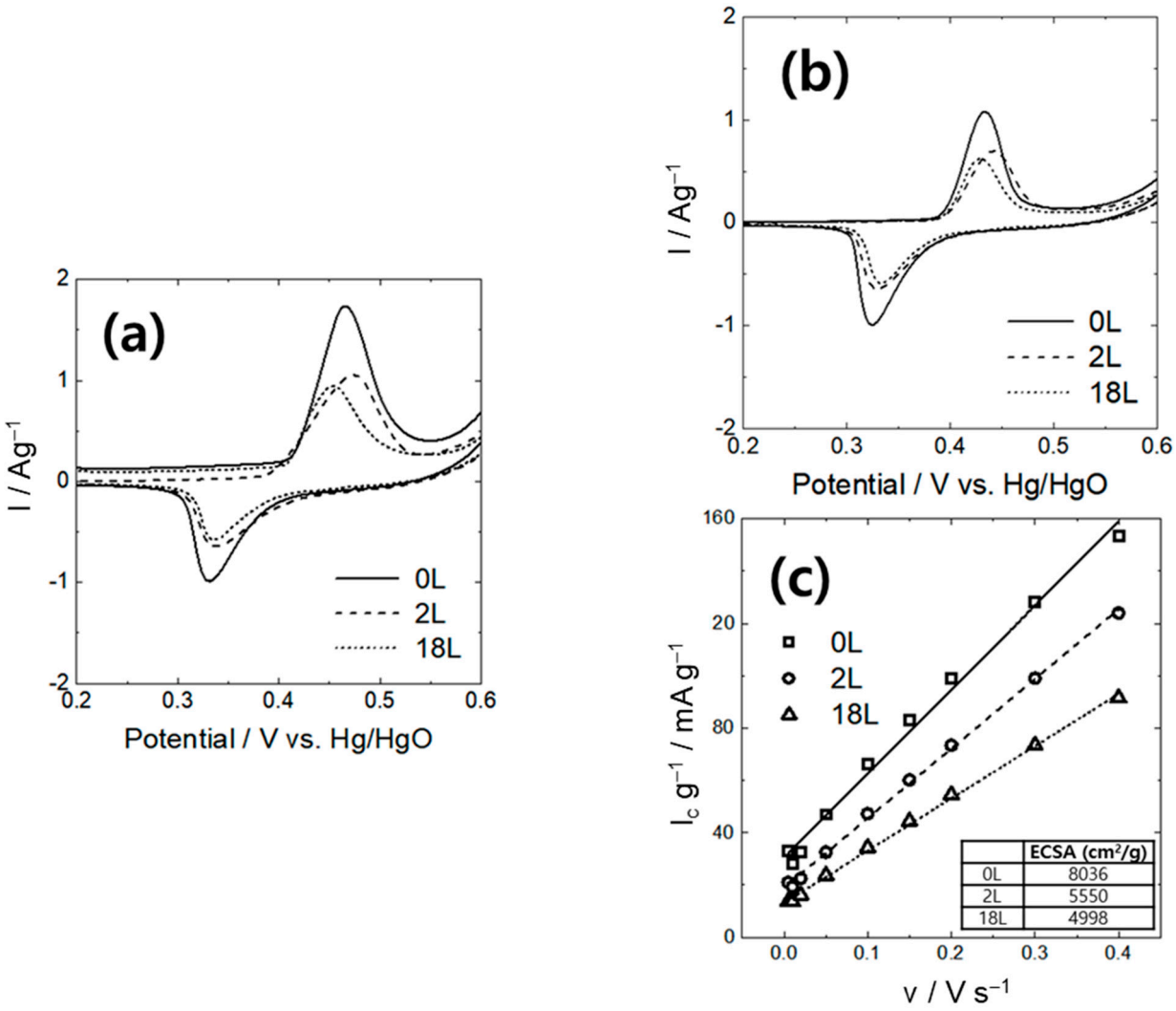

Figure 4. (**a**) The first and (**b**) the second cyclic voltammograms and (**c**) a charging current vs. scan rate plot (inset table is the estimated ECSA values), obtained from the nickel phosphide nanowires prepared at different values of magnetic field strength (Samples 0L, 2L, and 18L).

Figure 6 shows the rate characteristics of the cathodic reaction for the five specimens described above. First, in the case of the samples 0L, 2L, and 18L, which have the same phosphorus content, the larger the reaction surface area, the higher the cathodic charge amount value under a low rate (0.5 A/g) as described above. However, the specimen with a large surface area undergoes a relatively rapid decrease in the charge amount as the reaction rate increases (Figure 6a). For example, when sample 0L is compared with sample 18L, the charge amount, which showed a large difference at a low rate, becomes almost the same at 3 A/g. When the rate is further increased, sample 18L with a small

surface area shows a significantly higher charge amount. This tendency to achieve better rate characteristics with a small surface area can be confirmed more clearly through the charge amount retention plot (Figure 6b).

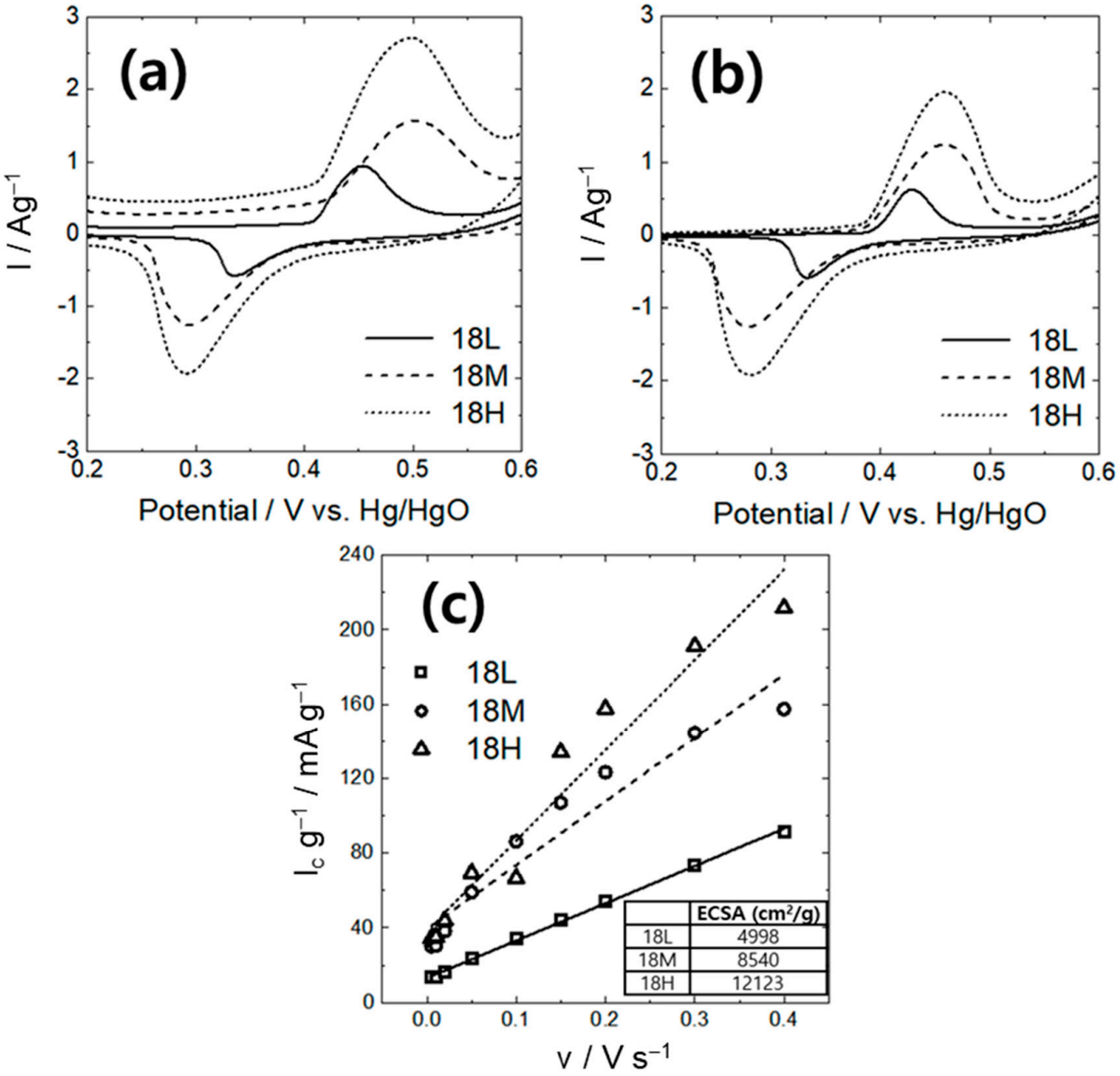

Figure 5. (**a**) The first and (**b**) the second cyclic voltammograms and (**c**) a charging current vs. scan rate plot (inset table is the estimated ECSA values), obtained from the nickel phosphide nanowires prepared at different combinations of pH and reducing agent content (Samples 18L, 18M, and 18H).

This unusual rate characteristic can be understood based on the nanowire shapes and pore structures of the electrodes (Figure 1). With regard to the nanowire shape, sample 0L is highly curved and, thus, has a high surface area; however, the electronic resistance might be large due to the complicated electron migration path and the severe contact between the nanowires. In contrast, sample 18L has a well-defined one-dimensional nanowire shape and has a very large aspect ratio, which results in relatively low electronic resistance. In addition, considering pore structure of the electrode constructed with nanowires, the apparent porosities of samples 0L, 2L, and 18L increased in order. Therefore, the open

pore structures lead to a decrease in migration resistance of active ions. Therefore, ohmic overpotential due to electronic and ionic resistance is expected to decrease in the order of samples 0L, 2L, and 18L. In other words, as the one-dimensional nickel phosphide nanowire is developed, a competitive situation arises, wherein the ohmic overpotential is decreased (due to the reduced electronic/ionic resistance) and the activation overpotential is increased (due to the reduced reaction surface area and increased reaction resistance). The experimental results (Figure 6) suggest that the well-developed nanowire specimen shows relatively good rate characteristics, indicating that the reducing effect of the ohmic overpotential outweighs the increasing effect of activation overpotential.

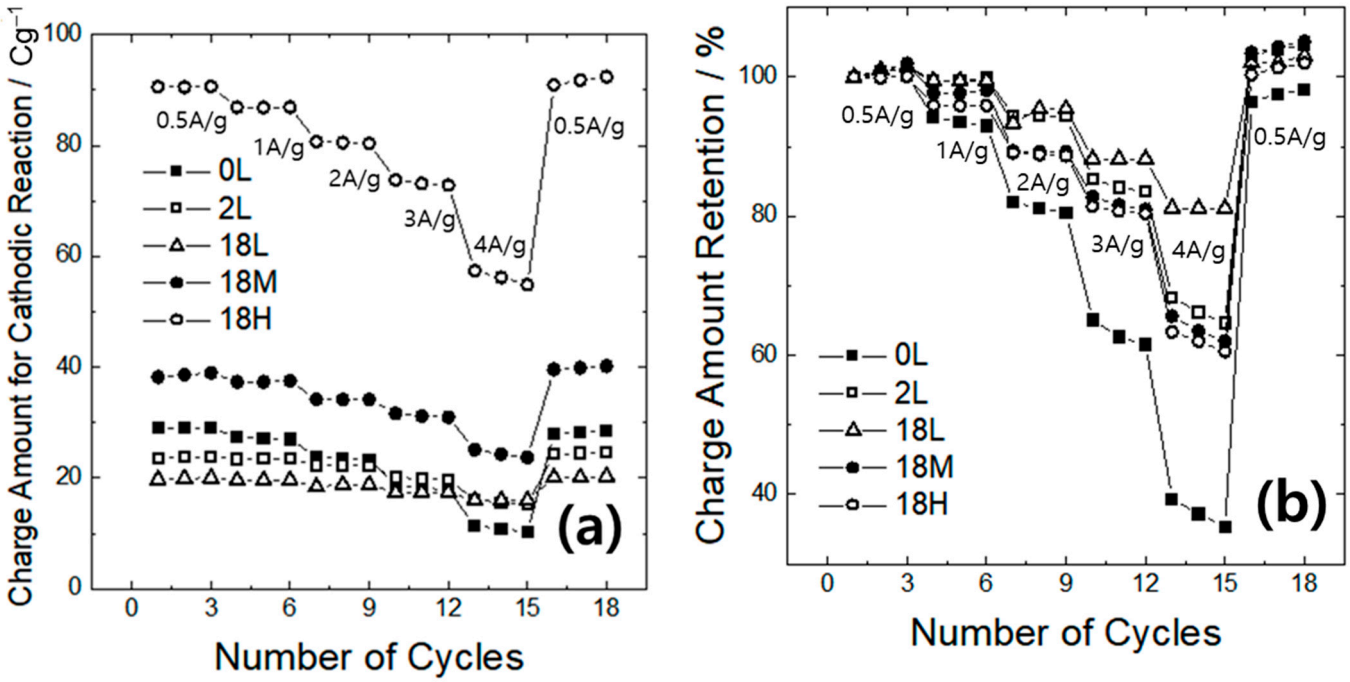

Figure 6. Rate characteristics of the samples. (**a**) Amount of cathodic charge amount and (**b**) charge amount retention at different cathodic current densities.

The rate characteristics of samples 18L, 18M, and 18H with different phosphorus contents also exhibit a similar trend, though the difference in charge amount retention is small between samples 18M and 18H. In fact, the surface reaction resistance or activation overpotential might be somewhat reduced because the reaction is more activated when the phosphorus content is high. Nevertheless, overall, sample 18L, which has a well-developed nanowire shape and an open pore structure, showed superior rate characteristics compared to sample 18M and sample 18H, which have relatively closed pore structures with small aspect ratios (Figure 3).

Figure 7 show the deterioration trend obtained for five specimens during the repetitive redox reaction cycles. Among the three electrodes with different phosphorus content (samples 18L, 18M, and 18H), sample 18H, which had the highest phosphorus content, showed the most significant deterioration, followed by sample 18M, which had a medium phosphorus content. Among the three electrodes with low phosphorus content (samples 0L, 2L, and 18L), the deterioration of sample 0L, which had the lowest phosphorus content and the least developed nanowire structure, was considerably high compared to the other two specimens (sample 2L and sample 18L) in which the nanowire structures were relatively well-developed. Therefore, it is considered that the higher the phosphorus content or the reaction surface area, the faster the rate of material deterioration due primarily to the greater amount of reacted nickel phosphide. The deterioration rate curve (Figure 7b) tells which phosphorus content or reaction surface area is relatively important degradation

factor: The robustness of sample 18L, which had the lowest values of both phosphorus content and surface area, was the best. It is noteworthy that the robustness of sample 0L, which had a low phosphorus content and a large response surface area, was significantly low. In contrast, the sample 18M, with a low surface area and middle phosphorus content, showed a relatively high robustness similar to those of samples 2L. This implies that the reaction surface area has a significant effect on the deterioration of the nickel phosphide nanowires compared to the phosphorus content.

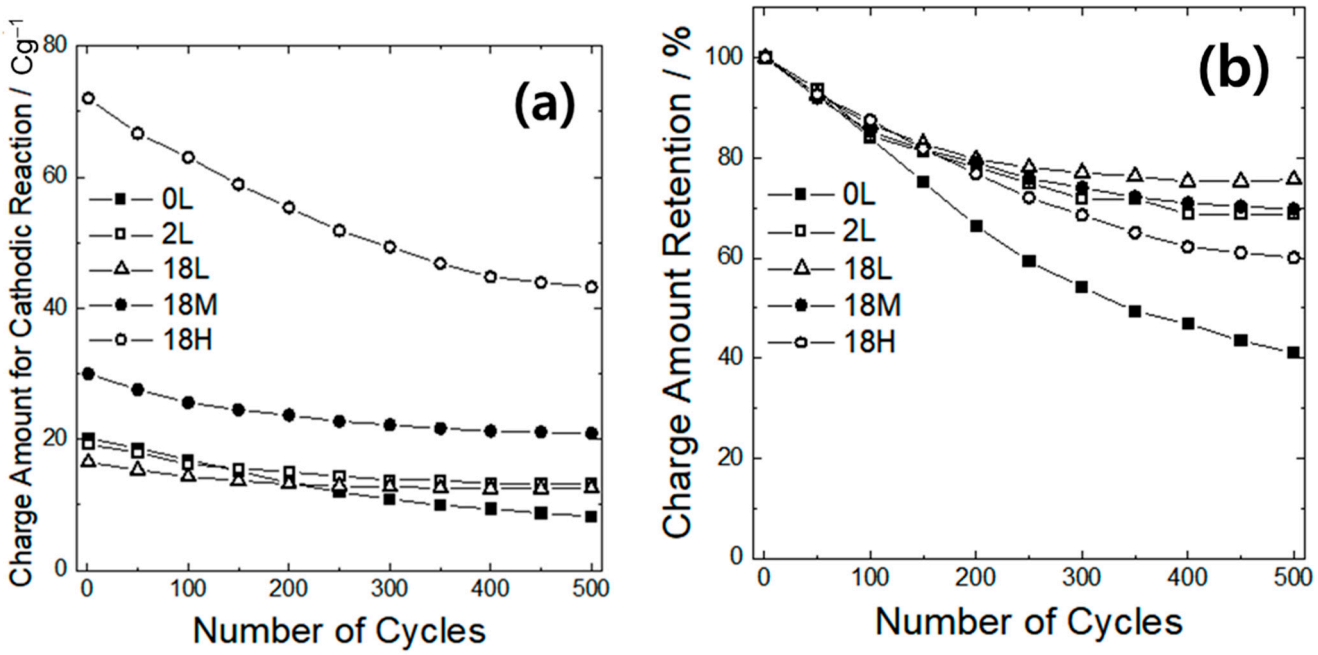

Figure 7. Variations of (**a**) the amount of cathodic charge amount and (**b**) charge amount retention with repetitive redox reactions.

4. Conclusions

In this study, nickel phosphide nanowires were fabricated using magnetically-assisted liquid phase synthesis for the first time, and specimens with different structures and phosphorus content were tested as electrodes for the electrochemical system. The experimental results are summarized as follows.

(1) Highly curved nanowires with low aspect ratios were formed without a magnetic field, while as the magnetic field strength increased, linear and well-defined nanowires with high aspect ratios were obtained. Under the same magnetic field strength, particles were agglomerated around the nanowire, and the aspect ratio tended to decrease as the phosphorus content in the nickel phosphide increased. Structural disturbance of the nanowire due to the increase in the phosphorus content might be caused by the decrease in magnetization due to the reduction of the nickel amount in the initial nanoparticles.

(2) When the phosphorus content in the nickel phosphide was the same, the reaction charge amount showed a general tendency proportional to the reaction surface area of the electrode. When the phosphorus content was increased, an additional increase in the reaction charge was observed. When the surface area effect was eliminated, the increase in reaction charge occurred solely due to the increase in the phosphorus content, indicating that reaction charge depends entirely on reaction surface area and phosphorus content.

(3) The rate characteristics increased when the surface area was small and the phosphorus content was low. An electrode consisting of curved nanowires with a low aspect ratio possessed large surface areas and, thus, might have low reaction resistance. However, the complex electron path and many contacts between the nanowires restricts the electron movement, and a relatively closed pore structure retards the ion movement. The unique

rate characteristics might appear because the increase in electron/ion migration resistance according to structural disturbance of the nanowire outweighs the decrease in surface reaction resistance.

(4) The electrode with a low surface area and low phosphorus content demonstrated the highest robustness against repetitive redox reactions, while an electrode with a low surface area and middle phosphorus content showed comparable robustness. In contrast, the robustness of the electrode having a low phosphorus content and large reaction surface area was significantly low. This suggests that reaction surface area is the dominant factor in nickel phosphide nanowire degradation compared to phosphorus content.

(5) The results of this study confirmed that the nickel phosphide nanowires can be easily controlled in structure and composition through chemical synthesis in a magnetic field and they have different characteristics in terms of reaction charge amount, rate characteristics, and robustness. The factors governing reaction kinetics and electrode degradation might give some insight into how to design nickel phosphide nanowires for specific applications. Various engineering applications can be possibly explored through a more extensive study on additional process factors such as surfactant concentration, including the process variables covered in this study.

Author Contributions: Conceptualization, formal analysis, investigation, data curation, writing—original draft preparation, H.-W.K.; writing—review and editing, supervision, project administration, funding acquisition, H.-C.S. All authors have read and agreed to the published version of the manuscript.

Funding: This work was supported by the National Research Foundation (NFR-2018R1A5A1025594) of the Ministry of Science and ICT, and was supported by the Materials Technology Institute at Pusan National University.

Data Availability Statement: The data that support the findings of this study are available on request from the corresponding author.

Conflicts of Interest: The authors declare no conflict of interest.

References

1. Feng, L.; Xue, H. Advances in Transition-Metal Phosphide Applications in Electrochemical Energy Storage and Catalysis. *ChemElectroChem* **2017**, *4*, 20–34. [CrossRef]
2. Parra-Puerto, A.; Ng, K.L.; Fahy, K.; Goode, A.E.; Ryan, M.P.; Kucernak, A. Supported Transition Metal Phosphides: Activity Survey for HER, ORR, OER, and Corrosion Resistance in Acid and Alkaline Electrolytes. *ACS Catal.* **2019**, *9*, 11515–11529. [CrossRef]
3. Theerthagiri, J.; Durai, G.; Karuppasamy, K.; Arunachalam, P.; Elakkiya, V.; Kuppusami, P.; Maiyalagan, T.; Kim, H.-S. Recent advances in 2-D nanostructured metal nitrides, carbides, and phosphides electrodes for electrochemical supercapacitors—A brief review. *J. Ind. Eng. Chem.* **2018**, *67*, 12–27. [CrossRef]
4. Carenco, S.; Portehault, D.; Boissière, C.; Mézailles, N.; Sanchez, C. Nanoscaled Metal Borides and Phosphides: Recent Developments and Perspectives. *Chem. Rev.* **2013**, *113*, 7981–8065. [CrossRef]
5. Li, X.; Elshahawy, A.M.; Guan, C.; Wang, J. Metal Phosphides and Phosphates-based Electrodes for Electrochemical Supercapacitors. *Small* **2017**, *13*, 1701530. [CrossRef]
6. Shi, Y.; Zhang, B. Recent advances in transition metal phosphide nanomaterials: Synthesis and applications in hydrogen evolution reaction. *Chem. Soc. Rev.* **2016**, *45*, 1529–1541. [CrossRef]
7. Weng, C.; Ren, J.; Yuan, Z. Transition Metal Phosphide-Based Materials for Efficient Electrochemical Hydrogen Evolution: A Critical Review. *ChemSusChem* **2020**, *13*, 3357–3375. [CrossRef]
8. Popczun, E.J.; McKone, J.; Read, C.G.; Biacchi, A.J.; Wiltrout, A.M.; Lewis, N.S.; Schaak, R.E. Nanostructured Nickel Phosphide as an Electrocatalyst for the Hydrogen Evolution Reaction. *J. Am. Chem. Soc.* **2013**, *135*, 9267–9270. [CrossRef]
9. Lu, Y.; Tu, J.P.; Xiang, J.Y.; Wang, X.L.; Zhang, J.; Mai, Y.J.; Mao, S.X. Improved Electrochemical Performance of Self-Assembled Hierarchical Nanostructured Nickel Phosphide as a Negative Electrode for Lithium Ion Batteries. *J. Phys. Chem. C* **2011**, *115*, 23760–23767. [CrossRef]
10. Du, W.; Kang, R.; Geng, P.; Xiong, X.; Li, D.; Tian, Q.; Pang, H. New asymmetric and symmetric supercapacitor cells based on nickel phosphide nanoparticles. *Mater. Chem. Phys.* **2015**, *165*, 207–214. [CrossRef]
11. Liu, M.-C.; Hu, Y.-M.; An, W.-Y.; Niu, L.-Y.; Kong, L.-B.; Kang, L. Construction of high electrical conductive nickel phosphide alloys with controllable crystalline phase for advanced energy storage. *Electrochim. Acta* **2017**, *232*, 387–395. [CrossRef]

12. Zhang, X.; Wu, A.; Wang, X.; Tian, C.; An, R.; Fu, H. Porous NiCoP nanosheets as efficient and stable positive electrodes for advanced asymmetric supercapacitors. *J. Mater. Chem. A* **2018**, *6*, 17905–17914. [CrossRef]
13. Xu, J.; Yang, N.; Yu, S.; Schulte, A.; Schönherr, H.; Jiang, X. Ultra-high energy density supercapacitors using a nickel phosphide/nickel/titanium carbide nanocomposite capacitor electrode. *Nanoscale* **2020**, *12*, 13618–13625. [CrossRef] [PubMed]
14. Mandel, K.; Dillon, F.; Koos, A.A.; Aslam, Z.; Jurkschat, K.; Cullen, F.; Crossley, A.; Bishop, H.; Moh, K.; Cavelius, C.; et al. Facile, fast, and inexpensive synthesis of monodisperse amorphous Nickel-Phosphide nanoparticles of predefined size. *Chem. Commun.* **2011**, *47*, 4108–4110. [CrossRef] [PubMed]
15. Zheng, X.; Yuan, S.; Tian, Z.; Yin, S.; He, J.; Liu, K.; Liu, L. Nickel/Nickel Phosphide Core−Shell Structured Nanoparticles: Synthesis, Chemical, and Magnetic Architecture. *Chem. Mater.* **2009**, *21*, 4839–4845. [CrossRef]
16. Rodriguez, J.A.; Kim, J.-Y.; Hanson, J.C.; Sawhill, S.J.; Bussell, M.E. Physical and Chemical Properties of MoP, Ni2P, and MoNiP Hydrodesulfurization Catalysts: Time-Resolved X-ray Diffraction, Density Functional, and Hydrodesulfurization Activity Studies. *J. Phys. Chem. B* **2003**, *107*, 6276–6285. [CrossRef]
17. Wang, K.; Yang, B.; Liu, Y.; Yi, C. Preparation of $Ni_2P/TiO_2-Al_2O_3$ and the Catalytic Performance for Hydrodesulfurization of 3-Methylthiophene. *Energy Fuels* **2009**, *23*, 4209–4214. [CrossRef]
18. Muthuswamy, E.; Brock, S.L. Solid-state phase transformations in solution: Templated conversion of nanoscale nickel phosphides. *Chem. Commun.* **2011**, *47*, 12334–12336. [CrossRef]
19. Duan, X.; Lieber, C.M. General synthesis of compound semiconductor nanowires. *Adv. Mater.* **2000**, *12*, 298–302. [CrossRef]
20. Lu, Y.; Wang, T.; Li, X.; Zhang, G.; Xue, H.; Pang, H. Synthetic methods and electrochemical applications for transition metal phosphide nanomaterials. *RSC Adv.* **2016**, *6*, 87188–87212. [CrossRef]
21. Shiomi, S.; Shamsuri, S.R.; Matsubara, E. Magnetic field strength controlled liquid phase syntheses of ferromagnetic metal nanowire. *Nanotechnology* **2020**, *31*, 365602. [CrossRef]
22. Wang, S.; Chen, K.; Wang, M.; Li, H.; Chen, G.; Liu, J.; Xu, L.; Jian, Y.; Meng, C.; Zheng, X.; et al. Controllable synthesis of nickel nanowires and its application in high sensitivity, stretchable strain sensor for body motion sensing. *J. Mater. Chem. C* **2018**, *6*, 4737–4745. [CrossRef]
23. Cossar, E.; Houache, M.S.; Zhang, Z.; Baranova, E.A. Comparison of electrochemical active surface area methods for various nickel nanostructures. *J. Electroanal. Chem.* **2020**, *870*, 114246. [CrossRef]
24. McCrory, C.C.L.; Jung, S.; Peters, J.C.; Jaramillo, T.F. Benchmarking Heterogeneous Electrocatalysts for the Oxygen Evolution Reaction. *J. Am. Chem. Soc.* **2013**, *135*, 16977–16987. [CrossRef]
25. Abrantes, L.M.; Fundo, A.; Jin, G. Influence of phosphorus content on the structure of nickel electroless deposits. *J. Mater. Chem.* **2001**, *11*, 200–203. [CrossRef]
26. Cortijo, R.O.; Schlesinger, M. Structural Studies of Electroless Thin Ni-P Films Grown in an Alkaline Environment. *J. Electrochem. Soc.* **1983**, *130*, 2341–2344. [CrossRef]
27. Kang, H.-K.; Shin, H.-C. Nickel Phosphide Electroless Coating on Cellulose Paper for Lithium Battery Anode. *J. Electrochem. Sci. Technol.* **2020**, *11*, 155–164. [CrossRef]
28. Loto, C.A. Electroless Nickel Plating—A Review. *Silicon* **2016**, *8*, 177–186. [CrossRef]
29. Wang, D.; Kong, L.-B.; Liu, M.-C.; Zhang, W.-B.; Luo, Y.-C.; Kang, L. Amorphous Ni–P materials for high performance pseudocapacitors. *J. Power Sources* **2015**, *274*, 1107–1113. [CrossRef]
30. Liu, S.; Sankar, K.V.; Kundu, A.; Ma, M.; Kwon, J.-Y.; Jun, S.C. Honeycomb-Like Interconnected Network of Nickel Phosphide Heteronanoparticles with Superior Electrochemical Performance for Supercapacitors. *ACS Appl. Mater. Interfaces* **2017**, *9*, 21829–21838. [CrossRef]
31. He, S.; Li, Z.; Mi, H.; Ji, C.; Guo, F.; Zhang, X.; Li, Z.; Du, Q.; Qiu, J. 3D nickel-cobalt phosphide heterostructure for high-performance solid-state hybrid supercapacitors. *J. Power Sources* **2020**, *467*, 228324. [CrossRef]
32. Agarwal, A.; Sankapal, B.R. Metal phosphides: Topical advances in the design of supercapacitors. *J. Mater. Chem. A* **2021**, *9*, 20241–20276. [CrossRef]
33. Saleh, A.A.; Amer, A.; Sayed, D.M.; Allam, N.K. A facile electrosynthesis approach of Mn-Ni-Co ternary phosphides as binder-free active electrode materials for high-performance electrochemical supercapacitors. *Electrochim. Acta* **2021**, *380*, 138197. [CrossRef]